INTERNATIONAL NUCLEAR SAFETY JOURNAL

ISSN 2285 – 8717
ISSN–L 2248 – 8717
http://www.insj.info

vol. 5 issue 2, 2016, pages 1 - 15

Using Enhanced Muon Tomography to Assess Core Relocation Following a Severe Reactor Accident

J. J. Bevelacqua
Bevelacqua Resources, 343 Adair Drive, Richland, WA 99352 USA
Corresponding author: bevelresou@aol.com

==========

Abstract
Muon tomography can reveal the location and configuration of a displaced core following a severe power reactor accident. The image contrast of this technique is enhanced using energies beyond those encountered in the cosmic ray muon spectrum. Optimum contrast is energy dependent and varies with the thickness of relocated core materials.

Keywords
Muon Tomography, Variable Energy Muon Beam, Power Reactor Accident Assessment, Image Contrast Optimization

==========

1.0 Introduction

Muon tomography [1-10] using the cosmic ray muon spectrum has been proposed and initially used as a methodology to determine the location of core materials in the damaged Fukushima Daiichi reactors [1-7]. To date, two primary core detection methods using cosmic rays muons have been proposed which are based on attenuation [1–3] and scattering [4–7]. Both methods are in their initial development phase and require significant optimization to reach their full potential. One enhancement to these methods is the use of muon energies beyond those encountered in a cosmic ray spectrum. In this paper, the attenuation approach is investigated using these higher energy muons.

The location of a displaced core has nuclear and radiological safety implications. In the case of the Three Mile Island Unit 2 (TMI-2) accident, core relocation had a significant impact on the defueling and nuclear safety requirements for reactor vessel activities [11]. This will also occur during the Fukushima Daiichi recovery activities.

At TMI-2 fuel debris was also displaced into the primary coolant system including the steam generators, pressurizer, make-up and purification demineralizer, and connecting piping systems. This relocation and the associated dose rates had a significant impact on the radiological controls implemented during the TMI-2 recovery [11]. Although fuel locations have not been completely mapped at the Fukushima Daiichi accident units, their position will dictate radiological and nuclear safety measures as the recovery proceeds. In general, fuel relocation following a severe accident depends on the accident sequence, availability of safety systems, and reactor vessel configuration [12].

The proposed muon tomography enhancement has the potential to assist recovery operations following reactor accidents involving core damage and relocation. It relies on the availability of a portable source to generate muons over a range of energies beyond those produced in a cosmic ray spectrum. Although this technology has yet to be fully developed, advances in electron accelerator technology suggest that it is achievable.

Small laser driven electron accelerators have been developed [13]. These accelerators are optical cavities that optimally have a size on the scale of the light's wavelength. Using shorter wavelength radiation increases the energy of these devices and with optimization GeV-TeV energies are feasible. Given the interaction similarities of muons and electrons, the advancement of the technology to generate muon beam sources is less of a technological step than the original laser accelerator development for electrons.

Technologies in development for the next generation electron accelerators and the development of muon-muon colliders also offer additional avenues for the technology assumed in this paper. Accordingly, this paper assumes portable muon accelerators are available and investigates their applicability in investigating core relocation events during a severe power reactor accident. Muon tomography also has applicability for special nuclear materials detection and in detecting uranium and plutonium cores of improvised or stolen nuclear devices. However, the present paper focuses on power reactor accident applications.

2.0 Muons and Their Interactions

Within the scope of the Standard Model of Particle Physics, electrons and muons are first and second generation leptons, respectively. Each lepton has unit charge, and the electron (muon) mass is 0.511 MeV (105.7 MeV) [14]. The Standard Model is reviewed from a health physics perspective and the relationship of muons and electrons within this model and their associated interactions are outlined in Ref. 14.

2.1 Muon Interactions

There are four basic interaction types [8-10] which determine the muon energy loss and generation of reaction products. These interactions are (1) ionization (including production of high energy knock-on electrons, or δ-rays), (2) direct production of electron-positron pairs, (3) bremsstrahlung, and (4) inelastic muon interactions with nuclei. The importance of the various interaction types vary with the incident muon energy and material being irradiated. These energy and material dependent features are complex and discussed in Refs. [8-10].

The muon interactions and their energy dependence [10] affect the calculation of quantities that influence the image produced through muon tomography. This is illustrated by calculating the contrast, stopping power, and range that are needed to assess the capability of muon tomography to distinguish fuel material from other materials found in a power reactor.

2.2 Contrast

The ability to distinguish various materials has been traditionally defined in medical imaging applications in terms of the contrast (C) [15]:

$$\mathbf{C = \frac{I_0 - I_1}{I_0}} \tag{1}$$

where I_0 is the intensity at a reference point and I_1 is the intensity at an adjacent location. This relationship is generalized to optimize and define an improved muon tomography process. In particular, contrast is defined in this paper as:

$$\mathbf{C_{ij}(x,E) = \frac{I_i(x,E) - I_j(x,E)}{I_i(x,E)}} \tag{2}$$

where $\mathbf{C_{ij}(x,E)}$ is the intensity of material j relative to material i at a distance x into each material at incident muon energy E, $\mathbf{I_i(x,E)}$ is the intensity in material i at location x and energy E, and $\mathbf{I_j(x,E)}$ is the intensity in material j at location x and energy E. This definition permits an assessment of the contrast as a function of energy and distance from a muon source.

The contrast defined in Eq. 2 permits optimization of the muon energy and source-detector distance to obtain an image of enhanced contrast. This optimized contrast facilitates determination of the location, shape, and extent of a displaced core following a severe reactor accident. In the case of Fukushima Daiichi, it would facilitate the assessment of the condition and location of the relocated cores in Units 1, 2, and 3.

To complete the Eq. 2 definition, the intensity is defined in a manner analogous to the absorbed dose delivered to a specific material. For a beam of muons having an initial energy E, the intensity as a function of penetration distance x is:

$$\mathbf{I(x,E) = \frac{1}{\rho}\left(-\frac{dE}{dx}\right)\Phi(x,E)} \tag{3}$$

where ρ is the density of the material attenuating the muon beam, -dE/dx is the stopping power, and Φ is the muon fluence. The muon fluence varies with penetration distance according to the relationship:

$$\mathbf{\Phi(x,E) = \Phi(0,E)\exp(-\mu x)} \tag{4}$$

where $\mathbf{\Phi(0,E)}$ is the entrance fluence and μ is the macroscopic reaction cross-section (linear attenuation coefficient). The linear attenuation coefficient is defined as

$$\mathbf{\mu = n\sigma} \tag{5}$$

where n is the number of atoms of absorbing material per unit volume and σ is the total microscopic reaction cross-section for the muon interaction. This interaction cross section is complex and addressed in Refs. 8-10. Cross-section data sets used in this paper were obtained using the methodology of Ref. 10. The next section of this paper outlines the calculation of the muon stopping power and range required to determine and intensity and associated contrast.

2.3 Stopping Power and Range

Most cosmic ray muons have energies below 10 GeV with the perk fluence occurring in the 1 – 3 GeV energy range [1 - 10]. These muons have been the primary source for power reactor tomography studies. A comparison of natural muon sources and variable energy beams is illustrated by investigating the stopping power and range of muons in various materials integral to a power reactor.

Using relativistic quantum mechanics, Bethe derived the following equation for the stopping power in a uniform medium for a charged particle [16-19]:

$$-\frac{dE}{dx} = \frac{4\pi k^2 z^2 e^4 n}{mc^2\beta^2}\left[\ln\frac{2mc^2\beta^2}{I(1-\beta^2)} - \beta^2\right] \quad (6)$$

where k is the electric constant, z is the muon charge, e is the magnitude of the electric charge, n is the number of electrons per unit volume in the medium interacting with the muons, m is the electron rest mass, c is the velocity of light in a vacuum, β is the velocity of the muon relative to the speed of light (v/c), v is the velocity of the muon, and I is the mean excitation energy of the medium interacting with the muons.

Using relativistic mechanics, β is determined from the total energy (W) and rest energy (E_o) [17 - 19]:

$$W = E + E_o \quad (7)$$

$$E_o = m_o c^2 \quad (8)$$

$$W = \frac{m_o c^2}{\sqrt{1-\beta^2}} \quad (9)$$

where E is the muon kinetic energy and m_o is the muon rest mass. Using Eqs. 7 – 9 leads to an expression for the kinetic energy:

$$E = W - E_o = m_o c^2\left(\frac{1}{\sqrt{1-\beta^2}} - 1\right) \quad (10)$$

Eq. 10 can be solved for β:

$$\beta = \left[1 - \left(\frac{m_o c^2}{E + m_o c^2}\right)^2\right]^{1/2} = \left[1 - \left(\frac{E_o}{W}\right)^2\right]^{1/2} \quad (11)$$

for use in Eq. 6.

The mean excitation energy I can be represented by the following empirical formulas for an element with atomic number Z [18]:

$$I \cong 19.0\,eV, Z = 1 \quad (12)$$

$$I \cong (11.2 + 11.72Z)\,eV, 2 \le Z \le 13 \quad (13)$$

$$I \cong (52.8 + 8.71Z)\,eV, Z > 13 \quad (14)$$

Once the stopping power is known, it is possible to calculate the muon's range. By definition, the range of a charged particle is the distance it travels before coming to rest. The reciprocal of the stopping power is the distance traveled per unit energy loss. Therefore, the range R(E) of a charged particle having kinetic energy E is the integral of the reciprocal of the negative stopping power from the initial kinetic energy E_i to the final kinetic energy of a stopped particle (E = 0):

$$\mathbf{R(E) = \int_{E_i}^{0} \left(dE / dx\right)^{-1} \, dE} \qquad (15)$$

Eq. 15 is often written in terms of the stopping power:

$$\mathbf{R(E) = \int_{0}^{E_i} \left(-dE / dx\right)^{-1} \, dE} \qquad (16)$$

Knowledge of the range is important because the tomographic image depends on the ability of the muon to reach the depth of interest. Both stopping power and range values are assessed using computational techniques.

The Stopping Powers and Ranges (SPAR) Code [20] is a FORTRAN program that computes the stopping powers and ranges for muons, pions, protons, and heavy ions in any nongaseous medium for energies up to several hundred GeV. Details of the SPAR Code are documented in Refs. [20-22]. SPAR includes a parameterization of the mean ionization energy, and the inclusion of shell-and density-effect corrections.

The SPAR results become less accurate above several hundred GeV. However, for the purposes of this paper, SPAR is sufficiently accurate to investigate muon tomography at energies below a few hundred GeV.

The stopping powers are calculated using the continuous slowing-down approximation (CSDA). Inherent in the CSDA is the exclusion of fluctuations of the energy loss. Therefore, the SPAR stopping powers correspond to the mean energy loss per unit path length resulting from collisions with electrons and, at very low energies, nuclear Coulomb scattering. The ranges do not include the effects of straggling and multiple Coulomb scattering. For stopping media composed of compounds or mixtures, the stopping powers are computed assuming the stopping effects for each element are additive.

3.0 Model Limitations

The proposed muon tomography model for ascertaining the location of a displaced core following a severe power reactor event has a number of inherent limitations. First, the model is limited to one dimension and provides no angular or scattering information. Second, the range of applicability is limited to muon energies of several hundred GeV. However, the model provides sufficient information to investigate the energy dependence of the muon tomography contrast or image resolution. In addition, the model produces specific muon tomography predictions for various core relocation configurations.

4.0 Range Results

Fig. 1 summarizes the results of range calculations for muon energies between 1 and 1000 GeV. The muon range increases with energy and compares closely with the results of Ref. 10 below several hundred GeV. At higher energies, the results differ by a factor of about 2 illustrating the limitations of the SPAR model [20] noted previously.

Using cosmic ray muon energies, iron and uranium are distinguishable, but the resolution achieved to date has not been optimized. In part, this explains the relatively poor resolution achieved in applications of muon tomography applied to core relocation events [1-7].

The next section of this paper investigates the impact of muon energy on the contrast in intensity between different attenuating media. Eqs. 2 – 4 are used to investigate factors that influence the image contrast of various materials to optimize the muon tomography technique for assessing core relocation events.

5.0 Contrast Results

The primary structural material in a light water reactor is steel and the fuel is primarily uranium dioxide (UO_2). Given the initial scooping calculations of this paper, steel is represented by iron. The contrast definition of Eq. 2 is applied to uranium dioxide and iron using the relationship:

$$\mathbf{C_{Fe,UO_2}(x,E) = \frac{I_{Fe}(x,E) - I_{UO_2}(x,E)}{I_{Fe}(x,E)}} \qquad (17)$$

As applied in Eq. 17, $\mathbf{I_{Fe}(x,E)}$ $\left(\mathbf{I_{UO_2}(x,E)}\right)$ is the intensity of a muon field of initial energy E after traversing a thickness x of Fe (UO_2). This is not the traditional contrast that measures the intensity in two adjacent regions. However, it reflects the relative intensity after the muons have traversed two different materials of thickness x. As defined in Eq. 17, the contrast provides a relative measure as a function of distance and energy of the intensity of muons at a specific distance in two different media. Large contrast values indicate good differential attenuation of muons and the possibility to optimize muon tomography. Optimum contrast is obtained for the C values of Eq. 1 that approach unity.

The contrast is determined for a range of x and E values. The x values are limited by the muon range and E is selected to correspond to various material thicknesses that could be encountered in a core relocation event. Therefore, a single muon energy will not produce optimum contrast between UO_2 and iron or water (H_2O) for all core relocation events. The material thicknesses involved in the relocation (e.g., UO_2, Fe, and H_2O) must be evaluated and optimized using appropriate energy muons.

Contrast results as a function or energy and materials are summarized in Tables 1 and 2. Table 1 (2) provides the contrast of UO_2 using iron (water) as the reference material for muon energy values of 1, 5, 10, 50, 100, and 500 GeV.

Table 1
UO_2 Muon Contrast with Respect to Iron

Distance into Material (cm)	Incident Muon Energy (GeV)					
	1	5	10	50	100	500
20	0.32	0.21	0.19	0.18	0.18	0.18
40	0.46	0.27	0.23	0.21	0.21	0.21
60	0.61	0.33	0.27	0.24	0.24	0.24
80	[a]	0.38	0.30	0.27	0.27	0.27
100	[a]	0.44	0.34	0.30	0.29	0.30
150	[a]	0.57	0.44	0.37	0.36	0.37
200	[a]	0.70	0.53	0.43	0.41	0.43
400	[a]	[a]	0.82	0.63	0.60	0.62
800	[a]	[a]	[a]	0.84	0.82	0.83
1000	[a]	[a]	[a]	0.90	0.88	0.88

[a] Range of muon in UO_2 is exceeded.

The results summarized in Tables 1 and 2 indicate that muon tomography yields a contrast that varies with energy, the specific medium attenuating the muons, and material thickness. This suggests that muon tomography can be optimized to facilitate the detection of a core relocation event. For a given material thickness, the Fe/UO_2 and H_2O/UO_2 contrast are optimized as the energy decreases. However, the muon must have sufficient energy to penetrate the material involved in the core relocation event. Therefore, the muon energy to optimize the contrast depends on the thickness of material produced during the relocation event. Thicker materials require a higher energy muon for muon tomography to be optimized. For example, material thickness values on the order of 80 cm or greater can not be reached by 1 GeV muons because these particles have insufficient range in UO_2 to reach this depth. Higher energies are required to image UO_2 material if its thickness exceeds 80 cm.

Based on Generation II and III reactor designs [12], a maximum UO_2 thickness of 200 – 500 cm would be created by a core relocation event. For UO_2 thicknesses of 200 – 500 cm, 10 – 50 GeV muons provide reasonable UO_2 contrast values with respect to iron (Table 1) or water (Table 2). These energies do not correspond to the most likely muon energies in a cosmic ray spectrum. Accordingly, localized muon sources with energies of 10 - 50 GeV have the potential to improve the contrast in muon tomography studies of a displaced core following a severe power reactor accident.

Table 2 repeats the calculations summarized in Table 1 for UO_2 relative to water as the reference material. The H_2O/UO_2 contrast is defined as:

$$\mathbf{C_{H_2O,UO_2}(x,E) = \frac{I_{H_2O}(x,E) - I_{UO_2}(x,E)}{I_{H_2O}(x,E)}} \qquad (18)$$

The H_2O/UO_2 contrast values suggest that muon tomography more readily distinguishes equivalent material thicknesses of UO_2 in a water background than UO_2 in an iron background (i.e., H_2O/UO_2 contrast is larger than Fe/UO_2 contrast) for the same x and E values. The energy and material thickness trends noted in Table 1 also appear in Table 2.

Table 2
UO_2 Muon Contrast with Respect to Water

Distance into Material (cm)	Incident Muon Energy (GeV)					
	1	5	10	50	100	500
20	0.62	0.49	0.44	0.39	0.37	0.36
40	0.81	0.61	0.53	0.44	0.41	0.40
60	0.92	0.71	0.61	0.50	0.44	0.43
80	[a]	0.78	0.68	0.54	0.48	0.47
100	[a]	0.84	0.73	0.58	0.51	0.50
150	[a]	0.93	0.84	0.67	0.58	0.57
200	[a]	0.98	0.91	0.75	0.65	0.63
400	[a]	[a]	0.995[b]	0.91	0.82	0.80
800	[a]	[a]	[a]	0.99	0.96	0.94
1000	[a]	[a]	[a]	0.997[b]	0.98	0.97

[a] Range of muon in UO_2 is exceeded.
[b] Three decimal places are listed for contrast values >0.99 to illustrate to approach of the contrast to unity.

Both water and iron contrast values are applicable to severe light water reactor accidents. The TMI-2 accident was a small break loss of coolant accident (LOCA) that involved fuel melting, but the reactor vessel remained intact. Core displacement occurred when melted fuel relocated to the lower reactor vessel head [11,17]. This configuration illustrates the Fe/UO_2 contrast condition. With an intact reactor vessel, muon tomography is not the best option for assessing the core location. Other options for determining the core geometry include video examinations through available reactor vessel penetrations, use of installed nuclear instrumentation, and radiation level measurements. In the case of TMI-2, a video examination was performed by accessing the core using a video camera inserted through a disassembled control rod drive mechanism [11]. The video examination revealed a debris bed and a depression about 1.5 m in depth suggesting fuel damage and relocation of a portion of the core from its initial location to the lower reactor vessel head region. As defueling proceeded, core relocation to the lower head was confirmed [11].

Muon tomography using water contrast is most applicable for a severe accident with associated failure of the reactor vessel and displacement of the core to an ex-vessel location. This situation is indicative of the Fukushima Daiichi accident with breaching of the reactor pressure vessel and primary containment vessel. In this situation, the core debris is likely partially or fully submerged in water and muon tomography represents a viable approach for determining its location and geometry.

For Fukushima Daiichi, access to the final core location is difficult since the upper reactor vessel head in a Boiling Water Reactor is solid metal. Other access points are available, but present a radiological challenge given the existing radiation levels in the reactor buildings of Units 1, 2, and 3.

The results of Tables 1 and 2 suggest there is a significant advantage to employing muon tomography with energies of 10 - 50 GeV. As demonstrated by current efforts [1-7], muon tomography resolution of a displaced core could be improved. This paper suggests a possible improvement by increasing the muon energy. As illustrated in Tables 1 and 2, the capability to distinguish fuel from other materials is improved at higher muon energies as the material thickness increases. An illustration of distinguishing fuel material following various core relocation events is illustrated in the next section.

6.0 Muon Tomography for Various Fuel Relocation Scenarios

The location of fuel following a severe core displacement event can be investigated using muon tomography. These conditions are investigated by assessing a generic reactor vessel /core configuration derived from the design data provided in IAEA-TECDOC-1120 [12]. Using the data from Ref. 12, the intact reactor vessel configuration with fuel is assumed to consist of the following generic structures that have been simplified to facilitate calculations within the one dimensional model utilized in this paper:

1. The reactor vessel shell is a 25 cm thick iron annulus which includes the various support components (e.g., baffle plates, core barrel, core support plates, core support columns, core former plates, and miscellaneous structural components).
2. A 40 cm annular water gap exists between the cylindrical core and the reactor vessel annulus inner wall.
3. The core is a 200 cm radius structure composed of UO_2. Melted fuel also has a UO_2 composition.

To assess accident conditions, a muon source is assumed to be positioned outside the outer reactor vessel annular wall and a detector is located 180^o opposite the source at the same elevation as the detector outside the vessel annulus. This geometry reduces the calculation to an effective one dimensional problem with various material configurations lying between the muon source and detector. Based on this configuration, 5 specific cases are evaluated. An incident muon energy of 50 GeV is used in subsequent calculations. This energy lies beyond most of the cosmic ray muon spectrum, and easily penetrates the material thicknesses used in the five cases defined in subsequent discussion.

The cases used in this paper are motivated by the TMI-2 defueling sequence and the accident scenarios that occurred at TMI-2 and Fukushima Daiichi. Since Fukushima Daiichi has yet to initiate vessel operations, using available TMI-2 defueling data is a reasonable choice [11].

At TMI-2, the damaged core configuration varied significantly as a function of axial position. At the top of the original core location, a severe depression existed and a rubble bed formed the displaced core surface. Although most the periphery of the core remained in its original location, the interior portions as well as some of the outer fuel assemblies melted.

The TMI-2 rubble bed consisted of damaged fuel, melted fuel, core debris, and structural members. Fused fuel assemblies, melted fuel assemblies, and solidified fuel resided below the debris bed. The lower reactor vessel head contained solidified fuel that relocated to that region after it had melted [11]. These conditions influence the selection of cases used in this paper.

In all of the following five cases, the 25 cm thick iron reactor vessel annulus remains intact. This provides 50 cm of iron between the muon source and detector.

6.1 Case 1

Case 1 is a complete core meltdown with no fuel or water remaining in the reactor vessel. This configuration consists of a voided 25 cm iron annulus. The Case 1 configuration would be indicative of a catastrophic core melt event that breaches the reactor vessel and the fuel melts through the lower vessel head and drains into the reactor building basement. Given the one dimensional model limitation imposed in the present paper, the muon source and detector lie at opposite sides of the voided 25 cm thick iron annulus.

6.2 Case 2

Case 2 is a core relocation event with fuel relocated to the lower head, but the reactor vessel remains intact. This scenario is similar to the TMI-2 accident with sufficient water remaining in the lower head to cool the melted fuel as it relocates to the bottom of the reactor vessel. Within the one dimensional model, the Case 2 configuration consists of a 25 cm thick iron annulus filled with a 480 cm diameter water cylinder.

6.3 Case 3

Case 3 is a core slump event where the fuel melts and fills the interior of the reactor vessel. This case includes an intact iron reactor vessel annulus. The annulus is filled with a 480 cm diameter cylinder of UO_2.

This case represents a slowly melting core with sufficient water inventory to prevent breaching of the reactor vessel. Case 3 is a slowly evolving TMI-2 event with sufficient water addition to protect the reactor vessel integrity.

6.4 Case 4

Case 4 is similar to Case 1, but the event produces a 25 cm annular thickness of UO_2 adhering to the inner wall of the reactor vessel. The event results in a breached reactor vessel with no water remaining in the vessel. Case 4 is similar to the TMI-2 accident that produced a layer of fuel next to the reactor vessel. However, Case 4 proceeds to the point of a breached vessel and a loss of all water inventory.

6.5 Case 5

Case 5 is similar to Case 4, but the vessel remains intact and is filled with water. The 25 cm UO_2 annulus is surrounded by the 25 cm vessel annular wall. This is a TMI-2 style event with most melting fuel relocated to the lower head. No vessel breach occurs which permits water to remain in the vessel.

7.0 Core Relocation Results and Discussion

The 5 core relocation events summarized in Table 3 suggest that muon tomography can distinguish severe core relocation event conditions based on the intensity of the transmitted radiation reaching the muon detector. Case 3 is the event that is readily detected within the one dimensional model based on the significant reduction in intensity. This intensity reduction is expected since a cylindrical slug of UO_2 resides within the reactor vessel annulus. Case 3 is clearly distinguished from the other cases, because its relative intensity is about an order of magnitude smaller that the other cases summarized in Table 3. In Table 3, the intensity relative to Case 1 is provided.

Table 3
Muon Tomography Characterization of Various Source-Detector Configurations within a Reactor Vessel

Case	Accident Description	Material Attenuating Muons[a]	Relative Intensity[b]
1	Complete core melt with fuel exiting the lower vessel head	50 cm iron	1.00
2	Core relocated to lower vessel head that remains intact	50 cm iron 480 cm water	0.817
3	Core slumps to fill all space to the reactor vessel inner wall.	50 cm iron 480 cm uranium dioxide	0.0713
4	Partial core melt with most fuel exiting the lower vessel head An annulus of UO_2 remains attached to an intact reactor vessel inner wall	50 cm iron 50 cm uranium dioxide	0.769
5	Partial core melt with most fuel relocated to the lower vessel head that remains intact An annulus of UO_2 remains attached to an intact reactor vessel inner wall	50 cm iron 430 cm water 50 cm uranium dioxide	0.640

[a]Material located between the muon source and detector within a one dimensional model.
[b]Relative to Case 1 intensity.

The voided reactor vessel configuration of Case 1 has the highest relative intensity (1.000). Case 2 is a reactor vessel filled with water and has a relative intensity which is smaller (0.817) than Case 1 because the void was replaced by water. In Cases 1 and 2, no fuel resides between the muon source and detector which yields the largest relative intensity values.

Cases 3, 4, and 5 involve UO_2 between the source and detector. These three cases are indicative of a core relocation event that results in a quantity of fuel remaining within the reactor vessel annulus. Case 4 is a breached reactor vessel with a 25 cm annular ring of UO_2 residing inside the vessel. In Case 4, no water inventory remains within the vessel. This case has a relative intensity of 0.769.

Case 5 is similar to Case 4, but the reactor vessel remains intact and filled with water inside the 25 cm UO_2 annulus. The Case 5 intensity (0.640) is smaller than Case 4, because the void is replaced by water.

The results of Cases 1-5 suggest that various core relocation events can be distinguished using muon tomography. Although the present calculations are one-dimensional, they suggest that further optimization in muon tomography methods are possible.

The Table 3 values are illustrative of the relative attenuation values that could result following a core relocation event. Although useful, these values become more meaningful when calibration data are available. These data include calibration curves representing intensity values as a function of muon energy and material thickness of iron, water, and uranium dioxide. When combined with site specific measurements that vary with location and muon energy, the calibration data provide the thicknesses of iron, water, and uranium dioxide that best fit the set of source-detector measurements. A sufficient number of measurements at various source-detector locations and muon energies generates the configuration of material thicknesses in a manner that is analogous to image formation using optical ray tracing [23].

The image resolution will depend on the accuracy and completeness of the calibration curves, available muon energy values, number of measurements, detector efficiency, and accessibility of areas for source and detector placement. However, the proposed approach provides the potential for an enhancement to currently available muon tomography approaches.

8.0 Conclusions

Muon tomography is an additional tool for assessing core relocation following a severe power reactor accident. Cosmic radiation muons are the source used in current experimental applications. Although these muons have provided initial first order measurements, improvements in image quality are possible using a higher energy muon source.

Based on initial calculations, higher energy muons have the potential to provide an improved image of the geometry and extent of a relocated core. This is achieved using various energy muons to reveal the configuration of fuel residing between the source and detector. The highest contrast values occur when UO_2 is surrounded by lower density material.

9.0 Acknowledgement

The author thanks Dr. Sergei Striganov of the Fermi National Accelerator Laboratory for providing muon cross section data sets for water, iron, and uranium dioxide.

10.0 Figure Caption

Fig. 1. Muon range as a function of energy for uranium, uranium dioxide, iron, and water. The range values are calculated using the SPAR code of Ref. 20.

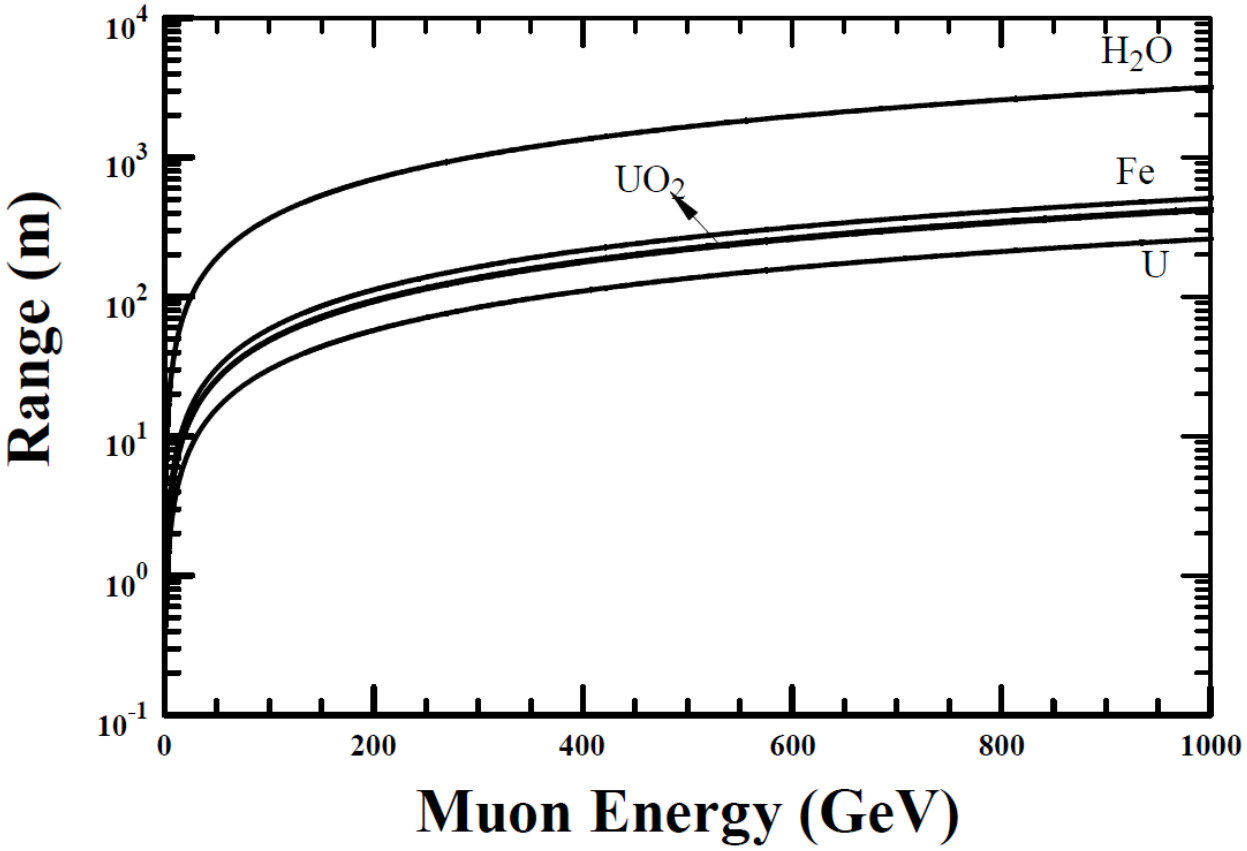

11.0 References

1. George EP. Cosmic Rays Measure Overburden of Tunnel. Commonwealth Engineer, 1 July, 455-457 (1955).
2. Alvarez LW, Anderson JA, Elbedwe F, Burkhard J, Fakhry A, Girgis A, Goneid A, Hassan F, Iverson D, Lynch G, Miligy Z, Moussa AH, Mohammed S, Yazolino L. Search for Hidden Chambers in the Pyramids, Science, 167, 832–839 (1970).
3. Nagamine K, Iwasaki M, Shimomura K, and Ishida K. Method of probing inner structure of geophysical substance with the horizontal cosmic ray muons and possible application to volcanic eruption prediction. Nucl. Instrum. Meth. A356, 585–595 (1995).
4. Borozdin KN, Hogan GE, Morris C, Priedhorsky WC, Saunders A, Schultz LJ, Teasdale ME. Radiographic imaging with cosmic-ray muons. Nature (London) 422, 277 (2003).

5. Morris CL, Alexander CC, Bacon JD, Borozdin KN, Clark DJ, Chartrand R, Espinoza CJ, Fraser AM, Galassi MC, Green JA, Gonzales JS, Gomez JJ, Hengartner NW, Hogan GE, Klimenko AV, Makela MF, McGaughey P, Medina JJ, Pazuchanics FE, Priedhorsky WC, Ramsey JC, Saunders A, Schirato RC, Schultz LJ, Sossong MJ, Blanpied GS, Tomographic Imaging with Cosmic Ray Muons. Science and Global Security 16, 37-53 (2008).
6. Schultz LJ, Borozdin KN, Gomez JJ, Hogan GE, McGill JA, Morris CL, Priedhorsky WC, Saunders A, Teasdale ME. Image reconstruction and material Z discrimination via cosmic ray muon radiography. Nucl. Instrum. Methods A519, 687-694 (2004).
7. Borozdin K, Greene S, Lukic´ Z, Milner E, Miyadera H, Morris C, Perry J. Cosmic Ray Radiography of the Damaged Cores of the Fukushima Reactors. Phys. Rev. Lett.109, 152501-1 - 152501-3 (2012).
8. Bogdanov AG, Burkhardt H, Ivanchenko VN, Kelner SR, Kokoulin RP, Maire M, Rybin AM, L. Urban L. Geant4 Simulation of High Energy Muon Interactions, Published in:Nuclear Science Symposium Conference Record. IEEE (Volume:4), 2043-2047 (2004), cern.ch/hbu/IEEE-TNS-01462665.pdf
9. Beatty J, Westerhoff S. The Highest-Energy Cosmic Rays. Annu. Rev. Nucl. Sci and Particle Physics 59, 319-345 (2009).
10. Groom DE, Mokhov NV, Striganov SI. Muon Stopping Power and Range Tables 10 MeV to 100 TeV. Atomic Data and Nuclear Data Tables 78 (2), 183-356 (2001).
11. GPU Nuclear letter, 4410-90-L-0012. Defueling Completion report, Final Submittal. General Public Utilities Nuclear Corporation, Middletown, PA (1990).
12. IAEA-TECDOC-1120. Assessment and management of ageing major nuclear power plant components important to safety: PWR pressure vessels. Vienna: International Atomic Energy Agency (1999).
13. Travish G, Yoder RB. Laser-powered dielectric-structures for the production of high-brightness electron and x-ray beams, in: K.W.D. Ledingham et al. (Eds.), Laser Acceleration of Electrons, Protons, and Ions; and Medical Applications of Laser-Generated Secondary Sources of Radiation and Particles, Prague, Czech Republic (SPIE, Bellingham, WA), Proceedings of SPIE, 8079, 80790K – 80790L (2011).
14. Bevelacqua JJ. Standard Model of Particle Physics-A Health Physics Perspective. Health Physics 99(5), 613– 623 (2010).
15. Johns EJ, Cunningham JR. The Physics of Radiology, 4th ed. Springfield, IL: Charles C Thomas (1983).
16. Bethe H. *Zur Theorie des Durchgangs schneller Korpuskularstrahlung durch Materie*. Ann. Phys. (Leipzig) 5, 325 - 400 (1930).
17. Bevelacqua JJ. Basic Health Physics: Problems and Solutions, 2nd ed. Weinheim: Wiley-VCH (2010).
18. Turner JE. Atoms, Radiation, and Radiation Protection, 3rd ed. Weinheim: Wiley-VCH (2007).

19. Marmier P, Sheldon E. Physics of Nuclei and Particles, Volume I. New York: Academic Press (1969).

20. Radiation Safety Information Computational Center Computer Code Collection: Code Package CCC-228 SPAR. Calculation of Stopping Powers and Ranges for Muons, Charged Pions, Protons, and Heavy Ions. Oak Ridge National Laboratory, Oak Ridge, TN (1985) , http://rsicc.ornl.gov.

21. Armstrong TW, Chandler KC. SPAR. a FORTRAN Program for Computing Stopping Powers and Ranges for Muons, Charged Pions, Protons, and Heavy Ions ORNL-4869. Oak Ridge National Laboratory, Oak Ridge, TN (1973).

22. Armstrong TW, Chandler KC. SPAR Stopping Powers and Ranges for Muons, Charged Pions, Protons, and Heavy Ions. Nucl. Instrum. Methods 113, 313-314 (1973).

23. Jenkins JA, White HE. Fundamentals of Optics, 3rd ed. New York: McGraw-Hill (1957).